Partitioning evapotranspiration in sparsely vegetated rangeland using a portable chamber

David I. Stannard[1] and Mark A. Weltz[2]

Received 12 May 2005; revised 18 November 2005; accepted 2 December 2005; published 22 February 2006.

[1] A portable chamber was used to separate evapotranspiration (*ET*) from a sparse, mixed-species shrub canopy in southeastern Arizona, United States, into vegetation and soil components. Chamber measurements were made of *ET* from the five dominant species, and from bare soil, on 3 days during the monsoon season when the soil surface was dry. The chamber measurements were assembled into landscape *ET* using a simple geometric model of the vegetated land surface. Chamber estimates of landscape *ET* were well correlated with, but about 26% greater than, simultaneous eddy-correlation measurements. Excessive air speed inside the chamber appears to be the primary cause of the overestimate. Overall, transpiration accounted for 84% of landscape *ET*, and bare soil evaporation for 16%. Desert zinnia, a small (~0.1 m high) but abundant species, was the greatest water user, both per unit area of shrub and of landscape. Partitioning of *ET* into components varied as a function of air temperature and shallow soil moisture. Transpiration from shorter species was more highly correlated with air temperature whereas transpiration from taller species was more highly correlated with shallow soil moisture. Application of these results to a full drying cycle between rainfalls at a similar site suggests that during the monsoon, *ET* at such sites may be about equally partitioned between transpiration and bare soil evaporation.

Citation: Stannard, D. I., and M. A. Weltz (2006), Partitioning evapotranspiration in sparsely vegetated rangeland using a portable chamber, *Water Resour. Res.*, *42*, W02413, doi:10.1029/2005WR004251.

1. Introduction

[2] The importance of evapotranspiration (*ET*) in the hydrologic cycle generally increases with increasing aridity [*Kurc and Small*, 2004]. In arid and semi-arid climates, *ET* often consumes a large part of precipitation, and the amount and timing of *ET* can strongly affect streamflow and groundwater recharge [*Decker et al.*, 1962; *Kurc and Small*, 2004]. Consequently, knowledge of *ET* rates and controlling factors in these settings can be an important part of understanding the hydrologic system. When dealing with mixed vegetation ecosystems, this knowledge ideally would extend to the various *ET* components (transpiration by species, soil moisture evaporation), providing a more detailed understanding of the surficial processes and relative rates of water use. However, micrometeorological or hydrologic methods to measure *ET* integrate over hectares or more, making discernment of individual components in a mixed canopy impossible. In these settings, chamber methods can be used to measure *ET* components and to help identify the factors controlling *ET* partitioning. The spatial resolution of the chamber methods can then be used with the temporal and spatial integration of the other methods to generate long-term, large-area estimates of *ET* components.

[3] Chambers are used to measure directly the flux of gases between the Earth's surface and the atmosphere by enclosing a volume and measuring all flux into and out of the volume [*Denmead et al.*, 1993]. Static chambers cover a portion of the land surface, either with or without vegetation, and flux from the surface is computed by measuring the change in gas concentration within the closed chamber during a short time [*Grau*, 1995]. Although the measurement is direct, the use of chambers often is criticized based on their potential to alter the natural environment of the vegetation or surface, thereby disturbing the measured flux [e.g., *Wagner and Reicosky*, 1992; *Denmead et al.*, 1993; *Dugas et al.*, 1997; *Heijmans et al.*, 2004]. Generally, static chamber measurements of *ET* are made quickly (seconds to minutes) to minimize this disturbance, but some disturbance generally remains. Often, chamber studies emphasize comparative (between sites) rather than absolute results, to largely remove the effects of measurement bias [e.g., *Pickering et al.*, 1993; *Decker et al.*, 1962; *Grau*, 1995; *Heijmans et al.*, 2004]. The use of chambers generally is labor-intensive or expensive, or both. Hence, a methodology to extrapolate chamber measurements in time and space could help answer questions related to *ET* partitioning in heterogeneous settings.

[4] The purposes of this paper are (1) to develop a methodology for estimating *ET* components at a mixed-vegetation rangeland site using a static chamber, (2) to assemble the components into an estimate of total landscape *ET* and compare it to an independent measurement, and (3) to investigate the factors controlling *ET* partitioning at the study site. A medium-sized (~0.7 m^3) static chamber is

[1]Water Resources Division, U.S. Geological Survey, Denver, Colorado, USA.
[2]Agricultural Research Service, U.S. Department of Agriculture, Beltsville, Maryland, USA.

Table 1. Physical Data and Average Latent-Heat Fluxes of Landscape Components

Common Name (Abbreviation[a])	Genus and Species	Height[b]	Relative Cover[c]	Fractional Cover[d]		Average Latent-Heat Flux			
						Component Scale[e]		Landscape Scale[f]	
				Value	Rank[g]	Value	Rank[g]	Value (%[h])	Rank[g]
Desert Zinnia (dz)	*Zinnia pumila*	0.1	0.145	0.114	2	773	1	88 (44%)	1
Bare Soil (bs)			1.000	0.737	1	44	7	32 (16%)	2
White Thorn (wt)	*Acacia constricta*	0.4	0.260	0.050	3	577	4	29 (14%)	3
Unmeasured Species[i] (us)				0.038	4	584	3	22 (11%)	4
Tar Bush (tb)	*Flourensia cernua*	0.4	0.290	0.024	6	730	2	18 (9%)	5
Creosote Bush (cb)	*Larrea tridentata*	0.9	0.382	0.029	5	312	6	9 (4%)	6
Mariola (ma)	*Parthenium incanum*	0.3	0.211	0.008	7	531	5	4 (2%)	7
Whole Landscape (ch)				1.0000				202 (100%)	

[a]Abbreviation of component common name, used as a superscript in this report.
[b]Height of individual shrub selected for chamber measurement (m).
[c]Relative cover (*RC*) is crown area of individual shrub selected for chamber measurement divided by area covered by chamber.
[d]Fractional cover (*FC*) is fraction of landscape covered by a component.
[e]Latent-heat flux of a component per unit plan area of component (shrub or bare soil), averaged over the study period (W m^{-2}).
[f]Latent-heat flux of a component per unit area of land surface, averaged over the study period (W m^{-2}), equal to fractional cover times component-scale latent-heat flux.
[g]A cardinal ordering of the magnitudes, arranged from greatest (1) to least (7).
[h]Percentage of average landscape latent-heat flux.
[i]Component-scale λE of unmeasured species set equal to mean of measured species.

used with a simple geometric model of the vegetated land surface to estimate landscape *ET*, transpiration from each of the five major species, transpiration from the remaining vegetation, and bare soil evaporation. We are not aware of any other study that has accomplished this in a mixed canopy. The chamber-based estimates of total *ET* are compared to simultaneous eddy-correlation measurements, and reasons for differences between them are discussed. Finally, changes in *ET* partitioning as a function of changes in the near-surface micro-climate are examined.

[5] Data collection took place during the Monsoon '90 multidisciplinary experiment, which was conducted in the Walnut Gulch experimental watershed, located in southeast Arizona, near the town of Tombstone. The watershed is monitored by the Southwest Watershed Research Center, part of the Agricultural Research Service, U.S. Department of Agriculture. Ground based and remote measurements of the surface energy balance, the hydrology, and many other aspects of the soil-plant-atmosphere continuum were made during the summer of 1990. These studies are documented in a special section of *Water Resources Research,* including an overview by *Kustas and Goodrich* [1994]. Monsoon '90 activities took place both before (June 4 to June 13) and during (July 18 to August 11) the monsoon season.

2. Materials and Methods

2.1. Study Area

[6] Chamber and eddy correlation (EC) measurements of *ET* were made at the Lucky Hills study site (METFLUX Site 1), which is within a dissected, sparsely vegetated subwatershed of Walnut Gulch (see *Kustas and Goodrich* [1994] for site map). The terrain is a series of nearly parallel ridges and washes running predominantly northeast to southwest, with adjacent ridges separated by about 200–600 m. Typical relief between adjacent ridges and washes is 10 to 20 m. The Lucky Hills study site was located on a relatively broad, flat ridgetop. The washes adjacent to the study site are separated from each other by about 500 m, and the nearly flat, level upland extends 200 m or more from the study site in the northeast (clockwise) through south directions, the direction of the prevailing wind during the study period.

[7] The vegetation is predominantly shrubs, about 1.2 m or less in height, punctuated occasionally by mesquite trees (*Prosopis juliflora*) and ocatillo (*Fouquieria splendens*), up to a few meters in height. Vegetation tends to occur in discrete clumps (one to a few shrubs per clump), with typically 2 to 5 m of bare soil between clumps. Live vegetation covered 26% of the land surface during the study [*Weltz et al.*, 1994], and fractional cover of the five dominant species is given in Table 1. Typical shrub height varies considerably, from about 0.1 m for desert zinnia to about 1 m for creosote bush. With the onset of the monsoon season, usually in mid-July, the vegetation canopy is transformed. Most species are leafless before the monsoon, and reach full leaf-out in a few weeks. During this period, leaf-area index (*LAI*) increases from near zero to around 1. While April, May, and June are the three driest months, about two-thirds of the annual precipitation occurs during the monsoon season (mid July through early September) [*Kustas and Goodrich*, 1994]. Volumetric soil water content in the top 5 cm was fairly constant at about 0.01 before the monsoon, and varied between about 0.01 and 0.17 during the monsoon. The soil is a gravelly loamy sand [*Kustas and Goodrich*, 1994], with a surface composed of 46% gravel [*Weltz et al.*, 1994].

2.2. Chamber Construction

[8] The chamber consists of an upper, hemispherical part (2.38-mm thick), and a lower, cylindrical part (3.18-mm thick), both made of Plexiglas G (Figure 1). These shapes were chosen to facilitate internal air circulation. Total height is 0.912 m, internal volume is 0.652 m^3, and the chamber covers a land-surface area of 0.898 m^2. The transmittance of the hemisphere to light is 92% at 0.375 μm and above. Two

Figure 1. Chamber operation in sparse canopy. Chamber being lowered over creosote bush. Eddy correlation sensors in left background.

12-volt high-speed fans were mounted inside the hemisphere to keep the air well mixed. A small wet-bulb, dry-bulb aspirated psychrometer (Model WVU, Delta-T Devices, Cambridge, England), was mounted inside the hemisphere with the intake at a height of 0.64 m above land surface, to record the change in wet- and dry-bulb temperature during a measurement. Further chamber construction details can be found in *Stannard* [1988].

2.3. Chamber Measurements

[9] Chamber measurements were made during daytime periods on August 1, 8 and 9, 1990. Shrubs of average size and vigor from each of the five dominant species (Table 1) were chosen to study. These were all single plants, except for desert zinnia, which was a group of six small plants. A bare soil site also was established. Sites were not replicated because the time needed to measure these 6 sites was nearly as long as the EC measurement interval (20 min), precluding a second round of chamber measurements. At some sites, the soil surface was graded slightly where it contacted the chamber edge, to obtain a good seal between the chamber and soil. The marks left on the soil surface by the chamber edge were used to return the chamber to the same location on successive measurements. Each measurement consisted of suspending the chamber, with fans running, about 1 m above land surface (to let the internal vapor density equilibrate with ambient), then lowering the chamber to the selected site (Figure 1), and recording internal wet- and dry-bulb temperatures with an electronic data logger every 2 s, for about 1 minute. A set, consisting of one measurement from each site, took about 12 to 15 min to complete. On August 1, sets were repeated at 15-min intervals. However, because the EC measurement interval was 20 min, the set interval was lengthened to 20 min on August 8 and 9 to facilitate comparison. Approximate simultaneity of August 1 data was achieved by averaging two consecutive chamber sets into a single set in two instances.

[10] Chamber data were processed with FORTRAN programs. Wet- and dry-bulb temperatures were converted into vapor pressure, e_{ch} (kPa), and vapor density, ρ_{vch} (g m^{-3}), using the standard psychrometric equation and the ideal gas law. A typical time series of ρ_{vch} during two measurements is shown in Figure 2. During the creosote-bush measurement, ρ_{vch} equilibrated with ambient air at about 10.7 g m^{-3}, began to increase when the chamber was lowered into position, and reached a maximum rate of increase 47 s after emplacement. The rate of increase slowed after this maximum because the internal air humidified, reducing the surface-to-air difference that drives *ET*. When the chamber was removed, ρ_{vch} decreased rapidly as the humid air was flushed from the chamber. The cycle was then repeated at the bare soil site, resulting in a much smaller maximum slope attained in a shorter time period (19 s).

[11] Latent-heat flux at each chamber site was computed using [*Stannard*, 1988]:

$$\lambda E_s = \lambda MVC/A \tag{1}$$

where λ is the latent heat of vaporization of water (J g^{-1}), E_s is the evapotranspiration rate from a site, (g m^{-2} s^{-1}), λE_s is latent-heat flux from a site (W m^{-2}), M is the maximum slope of the vapor density time series (g m^{-3} s^{-1}), V is the volume of the chamber (m^3), C is the calibration factor of the chamber (unitless), and A is the area of land surface covered by the chamber (m^2). Because λ is virtually constant over the range of temperatures encountered in this study, λE is used here to quantify *ET*, in order to facilitate comparison with other components of the surface energy balance (100 W m^{-2} = 0.0412 g m^{-2} s^{-1} = 3.56 mm d^{-1} at 30°C, the mean chamber temperature during the study). The

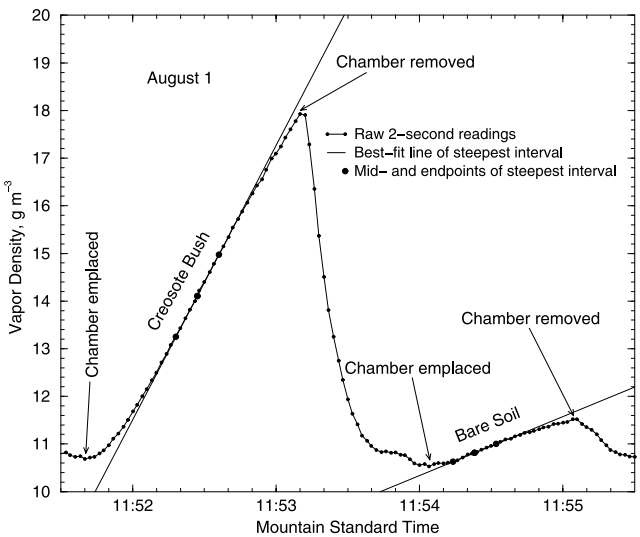

Figure 2. Time series of vapor density during two consecutive measurements showing best fit lines, midpoints, and endpoints of steepest intervals.

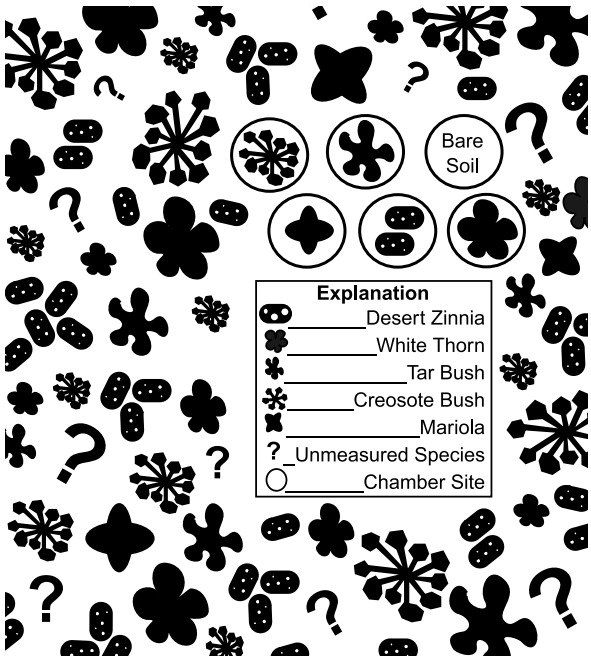

Figure 3. Conceptual model of sparse, heterogeneous canopy. Shrubs are represented as they would appear in an aerial photograph. White background represents bare soil.

slope of the vapor-density time series was calculated using ordinary least squares on successive 10-point intervals of the time series. The interval was numerically advanced through each time series by 1-point increments, and the steepest slope was retained as M (the slope of the lines in Figure 2). The measurement is assigned the time t_m, corresponding to the midpoint of the steepest interval.

[12] Chamber calibration consisted of evaporating water from a beaker at a known rate, emplacing the chamber over the beaker, and comparing the rate measured by the chamber (using a 10-point interval and assuming a temporary value of $C = 1$) to the known rate [*Stannard*, 1988]. This was repeated over a range of rates, and the measured rates were plotted against the known rates. The calibration factor of the chamber, C, was equal to the slope of the best fit line through the origin. The calibration factor, in this case equal to 1.136, accounts for the overall response time of the chamber, psychrometer errors, and adsorption of water vapor by the chamber wall.

2.4. Canopy Model

[13] Site *ET* rates calculated using equation (1) are composed of transpiration from a specific shrub of a specific size, and evaporation from bare soil (or just bare soil evaporation in the case of the bare soil site). Quantification of more useful generalized fluxes requires the use of a model that accounts for the size of the shrubs at each measurement site and the relative abundance of each species in the canopy. A simple patchwork geometric model [*Stannard*, 1988] is used to separate each site measurement into transpiration and soil evaporation within the chamber, and to then reassemble these into canopy fluxes based on fractional-cover data.

[14] The multi-component, one-layer model used here represents a sparse canopy as a planar surface, similar to an aerial photograph of the surface. The model quantifies the small-scale heterogeneity associated with plant size, spacing and diversity, but is homogeneous on a landscape scale. The surface is divided into many small polygons, of several different types, with a background between the polygons (Figure 3). Each shrub polygon is defined by the crown area of that shrub, or the vertical projection of the shrub perimeter. Each type represents a species and the background represents bare soil between shrubs. Together, the species types and bare soil comprise the components of the landscape. At any given time, *ET* is allowed to vary between components, but is assumed to be constant within a component. Soil evaporation occurring from within the crown area is not explicitly quantified, but is included in the transpiration from the shrub. *ET* from species not measured in the chamber is assumed to be equal to the mean *ET* from the measured species.

[15] A system of superscripts and subscripts is used to designate components and measurement scale, respectively. Each component superscript consists of a two-letter abbreviation of the common name, given in Table 1. Fluxes are discussed at site, component, and landscape scales, subscripted "s", "c" and "l", respectively. Site fluxes are the raw field measurements, which generally include both transpiration and bare-soil evaporation (the exception is the bare-soil site). Component-scale fluxes are expressed per unit area of that component, and landscape-scale fluxes are expressed per unit area of land surface. Mathematically, the canopy model can be written [*Stannard*, 1988]:

$$\lambda E_{ch} = \sum_{i=1}^{n} \frac{FC^i\left[\lambda E_s^i - \lambda E_s^{bs}(1 - RC^i)\right]}{RC^i} + FC^{us} \sum_{i=1}^{n} \frac{\lambda E_s^i - \lambda E_s^{bs}(1 - RC^i)}{n \cdot RC^i} + FC^{bs}\lambda E_s^{bs} \quad (2)$$

where λE_{ch} is the chamber value of total landscape-scale latent-heat flux (W m^{-2}), i is an index representing each of the measured species, n is the number of measured species, FC^i is fractional cover of the ith species, λE_s^i is the site latent-heat flux from the ith species (W m^{-2}), λE_s^{bs} is the site latent-heat flux from bare soil (W m^{-2}), RC^i is relative cover of the individual shrub chosen to represent the ith species (crown area divided by chamber area, unitless), FC^{us} is fractional cover of the unmeasured species and FC^{bs} is fractional cover of bare soil. All values of FC and RC are expressed as a number between 0 (no cover) and 1 (full cover). Equation (2) provides landscape-scale estimates of transpiration from each of the measured species [the first term on the right-hand side (rhs) of equation (2), with appropriate superscript], transpiration from all of the unmeasured species (the second term on the rhs), total transpiration (sum of the first two terms on the rhs), bare soil evaporation (the third term on the rhs) and total *ET* (the left-hand side). Dividing the landscape values by the appropriate FC yields the component-scale fluxes (W m^{-2} of component).

2.5. Eddy Correlation Measurements

[16] Landscape-scale eddy-correlation measurements of latent-heat flux, λE_{ec}, and sensible-heat flux, H_{ec}, were made during all chamber measurements at 20-min intervals, using a Campbell, Scientific CA27 sonic anemometer and KH20 krypton hygrometer, deployed at a height of 2.0 m.

The EC method and data processing are described in *Stannard et al.* [1994]. Source-areas of the EC sensors were computed following *Schuepp et al.* [1990] using a roughness length, z_o, and zero-plane displacement, d, of 0.04 m, and 0 m, respectively [*Stannard et al.*, 1994], and measured values of wind speed and wind direction (section 2.6). The surface layer was slightly to moderately unstable during the chamber measurements ($-0.5 < z/L < -0.025$, where z is the EC sensor height and L is the Obukhov length). Using these inputs, 84% to 100% of the EC source area was contained within the relatively flat, broad, homogenous ridgetop surrounding the chamber and EC sensors (Figure 1). Therefore the vegetation characteristics and resulting *ET* of the areas sampled by the two methods should be relatively similar, even though the EC method sampled a much larger area.

2.6. Other Measurements

[17] Fractional cover (*FC*) was measured at the study site [*Weltz et al.*, 1994] using the line-intercept method [*Canfield*, 1941]. Data from five parallel 30.5-m transects were averaged to obtain the mean *FC* of the landscape (Table 1). Relative cover (*RC*) of each chamber-site shrub was determined from birds-eye photos of each measurement site, taken from about 3 m above the ground. The circular impression in the soil made by the chamber edge was used as an indication of chamber area. The images were cut into vegetation and soil regions, and weighed on a sensitive balance (resolution = 0.1 mg) to determine raw values of *RC*. The raw values were corrected to account for parallax using the camera height of each photo.

[18] Volumetric soil water content (m^3 water m^{-3} soil, here unitless) at a depth of 2.5 cm, $\theta_{2.5}$, was measured every 10 s using resistance sensors, and 20-min averages were recorded. The mean output of 12 sensors was calibrated against gravimetric samples collected daily of the top 5 cm of soil, converted to volumetric using measured bulk density [*Schmugge et al.*, 1994]. Soil water content also was measured daily (~9:00) at greater depths (5, 10, 15, 20, 30, and 50 cm) using time-domain reflectometry (TDR) [*Goodrich et al.*, 1994]. The means of 6 replicates at each depth are designated θ_j, where j is the measurement depth in cm.

[19] Net radiation at a 1.66-m height, R_n (W m^{-2}), was measured every 10s and averaged over 5-min intervals, using a REBS Q*6 net radiometer [*Stannard et al.*, 1994]. Another measurement of net radiation was made at a 3.3-m height, using the same model sensor [*Kustas et al.*, 1994]. The higher sensor more effectively averaged across the scale of heterogeneity defined by the shrub spacing [*Reifsnyder*, 1967], but means were only recorded every 20 min. Twenty-min means from the two sensors were nearly identical. Because of our interest in the 5-min resolution, we use data from the lower sensor in this study. Soil-heat flux, G (W m^{-2}), was measured every 20 min using the combination method [*Fuchs and Tanner*, 1968]. Three pairs of heat flow transducers and averaging thermocouples were deployed in different shading conditions and weighted according to fractional cover data. Details of soil-heat flux computations are given in *Stannard et al.* [1994].

[20] Standard weather data were measured every 10 s and averaged over 20-min intervals. These data included air temperature at 2.0 m, T_2 (°C); relative humidity at 2.0 m, rh_2 (unitless); wind speed, u_4 (m s^{-1}), and wind direction, Az_4 (°), at 4.25 m; and solar radiation (W m^{-2}) [*Kustas et al.*, 1994]. Vapor pressure, e_2 (kPa), and vapor pressure deficit, VPD_2 (kPa), at a 2.0-m height were calculated from T_2 and rh_2 using standard equations. Soil-surface temperature, T_{ss} (°C), was measured on the same schedule at the weather data using an infrared thermometer. Rainfall was measured using a weighing, recording rain gage.

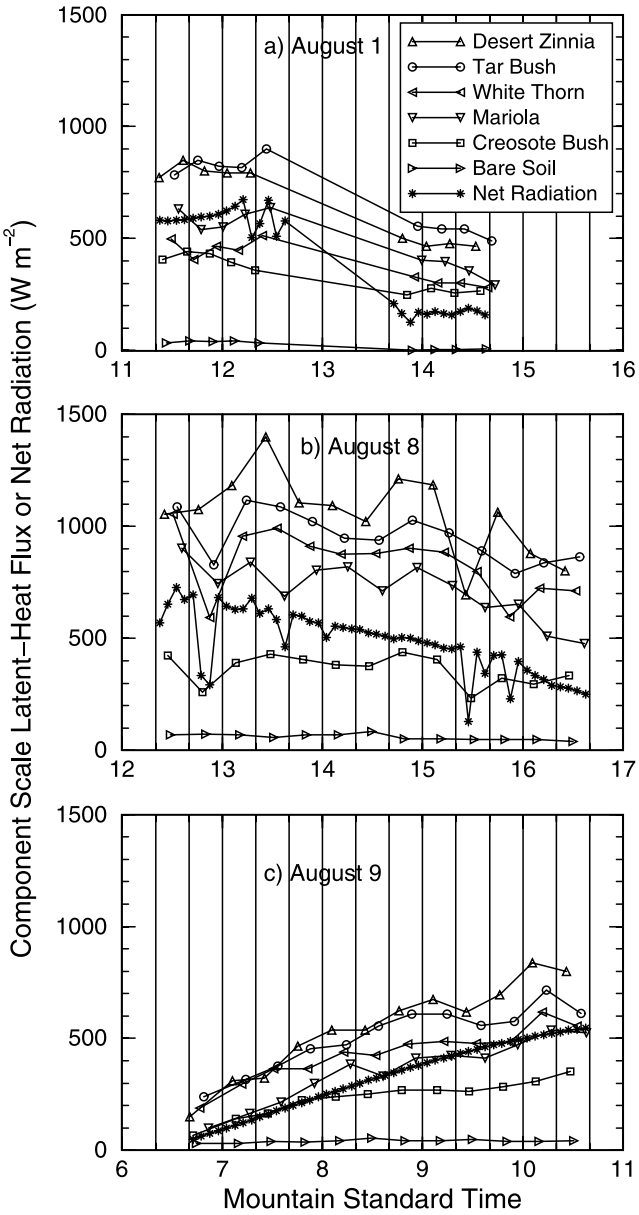

Figure 4. Chamber component-scale (per unit plan area of component) latent-heat flux and net radiation on (a) August 1, (b) August 8, and (c) August 9.

3. Results

[21] Time series of component-scale latent-heat fluxes, λE_c^i, and net radiation, R_n, are shown in Figure 4. All measurements are plotted at the midpoints of their intervals. At this location and time of year, solar noon occurs at 12:26 Mountain Standard Time. The morning of August 1 began with clear skies, became partly cloudy around noon, and

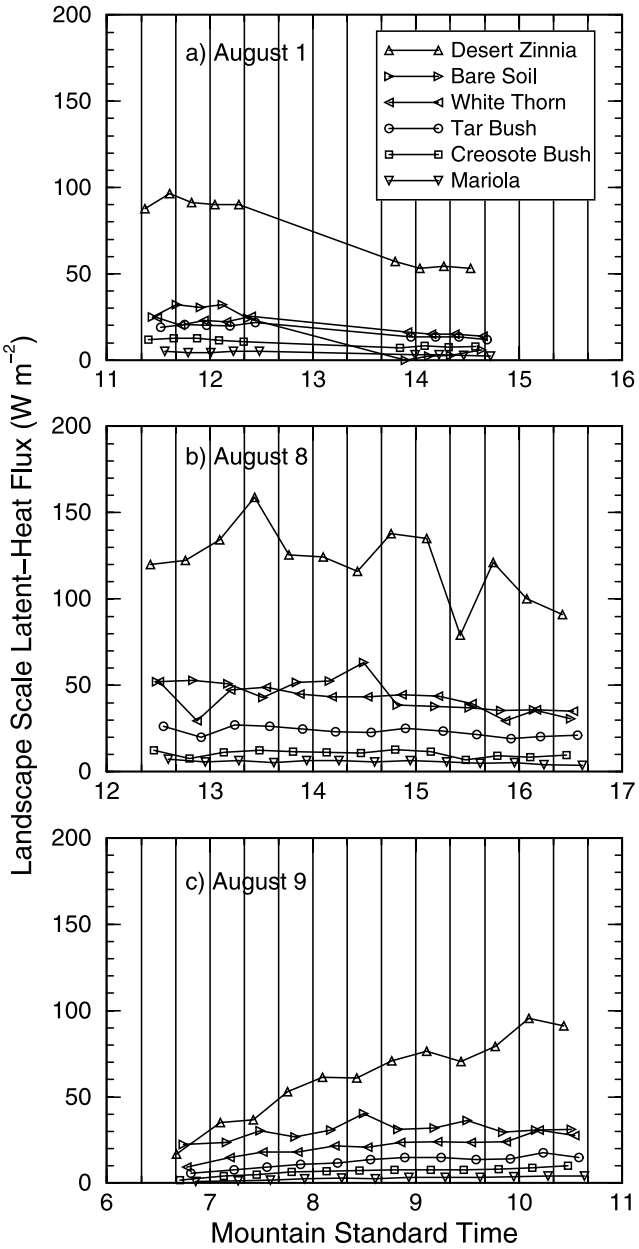

Figure 5. Chamber landscape-scale (per unit area of land surface) latent-heat flux by component on (a) August 1, (b) August 8, and (c) August 9.

was fully overcast by afternoon (Figure 4a). August 8 alternated between partly cloudy and clear (Figure 4b), and August 9 was completely clear (Figure 4c). The soil surface was dry and near-surface soil moisture, $\theta_{2.5}$, was relatively low on all 3 days (0.0141 ± 0.0010 on August 1, 0.0468 ± 0.0006 on August 8, and 0.0441 ± 0.0017 on August 9). In contrast, soil moisture from 10 cm to 50 cm was ample (0.10–0.19) during the study. Both the diurnal cycle (from 6:40 to 16:40) and variable cloudiness contributed to the wide range in R_n (50 to 728 W m^{-2}) measured during the study. In general, λE_c^i tends to follow the patterns of R_n (Figure 4), but the two are only moderately correlated.

[22] During partly cloudy periods, R_n sometimes fluctuated substantially on a 5-min basis (Figures 4a and 4b). The resulting effect on λE_c is evident in Figure 4b, where several dips in 5-min R_n are reflected in the chamber fluxes most concurrent with the brief cloud cover (e.g., the R_n periods beginning 12:45, 12:50, 13:35, 15:25 and 15:50 on August 8). However, some erratic fluctuations in R_n do not correspond to fluctuations in any λE_c (e.g., R_n period beginning 12:15 on August 1) and some erratic fluctuations in λE_c do not correspond to fluctuations in R_n (e.g., desert zinnia points at about 13:26, 14:45, 15:06 and 15:45 on August 8). In partly cloudy conditions, even 5-min R_n data do not fully capture the variability affecting the very short (~30 s) chamber measurements [*Pickering et al.*, 1993]. Bare soil evaporation, λE_c^{bs}, was affected less than the other components by short-term changes in R_n (Figures 4a and 4b). The dry soil surface filtered out rapid changes in energy supply to the moister soil layers below, where evaporation took place. Short-term fluctuations also occurred in some of the chamber fluxes during the clear day, August 9, and cannot be explained by corresponding changes in R_n (Figure 4c). Patterns in other factors that affect *ET* (temperature, vapor pressure, vapor-pressure deficit, wind speed; not shown) also do not explain the variations in the chamber fluxes. These erratic fluctuations probably are an indication of the random noise inherent in the chamber method.

[23] Vegetative λE_c typically was quite large and varied by about a factor of 2 to 3 between species near midday (Figure 4). Average values of λE_c^i and ranks are given in Table 1. Desert zinnia and tar bush stand out as the greatest component-scale water users (above 700 W m^{-2} on average) and creosote bush stands out as the least. The species tended to maintain rank relative to one another, but exceptions did occur, especially during partly cloudy conditions (Figure 4b). As a result of the dry soil surface, λE_c^{bs} was much smaller than vegetative λE_c, and was less variable with time.

[24] Time series of landscape-scale latent-heat fluxes, λE_l^i, during the 3 study days are shown in Figure 5, and average values and ranks are given in Table 1. At this scale, desert zinnia was by far the greatest water user, a result of its greatest component-scale *ET* and its greatest vegetative fractional cover (*FC*). The relative importance of bare soil evaporation increased dramatically at the landscape scale due to its large *FC* (0.737). Although the soil surface was dry, landscape-scale soil evaporation was second only to desert zinnia transpiration. The range in λE_l among the five dominant species was more than one order of magnitude; much larger than the range in λE_c (a factor of 2 to 3). All components maintained rank relative to one another from day to day, except for soil evaporation. On the afternoon of August 1, when clouds of an approaching storm moved in, soil evaporation decreased drastically, dropping it to third in importance for the day. Overall, transpiration accounted for 84% of *ET* and soil evaporation for 16%.

[25] Landscape-scale latent-heat fluxes by component are plotted against total landscape latent-heat flux, λE_{ch}, in Figure 6. In general, the individual components are roughly proportional to λE_{ch}, as indicated by their near-zero Y intercepts (from −5.25 to 2.89 W m^{-2}) and relatively high linear correlation coefficients (r = 0.79 to 0.98). This approximate proportionality instills confidence in the chamber method and implies that *ET* partitioning among components did not vary widely during the study. Considering that

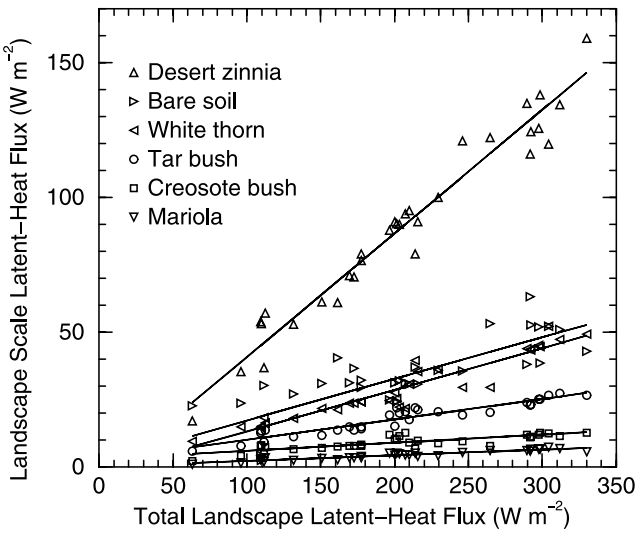

Figure 6. Landscape-scale latent-heat fluxes by component as a function of total landscape latent-heat flux, with best fit lines.

the soil surface was dry, $\theta_{2.5}$ was less than 0.048, and that root-zone soil moisture was ample, this relatively constant partitioning is reasonable.

[26] Time series of 20-min landscape-scale chamber and EC latent-heat fluxes, λE_{ch} and λE_{ec}, respectively, and net radiation, R_n, are shown in Figure 7. All measurements are plotted at the midpoints of their intervals. Most of the short-term variability in R_n and chamber *ET* during partly cloudy times (Figure 4) disappears on a 20-min basis. Averaging six site measurements into each 20-min chamber flux effectively removes much of the susceptibility to partial cloudiness evident in Figure 4, that concerned *Pickering et al.* [1993]. The resulting λE_{ch} is well correlated with R_n and λE_{ec} on each day, establishing confidence in the chamber methodology during partly cloudy conditions as long as measurements are made frequently. The chamber and EC methods clearly track changes in *ET* similarly, but the chamber method tends to overestimate flux compared to EC. In addition, the difference between the two varied over time and was greatest on August 8.

[27] A direct comparison of λE_{ch} and λE_{ec} is shown in Figure 8. The two measurements were highly correlated on each of the 3 days. The correlation coefficient, *r*, is 0.98, 0.93, and 0.95 on August 1, 8, and 9, respectively. The overall *r*, 0.92, is smaller than the daily *r* values, primarily because the systematic bias varied from day to day, especially on August 8. The ratio of λE_{ch} to λE_{ec} is 1.19, 1.37, and 1.14 on August 1, 8, and 9, respectively, and the overall ratio of λE_{ch} to λE_{ec} is 1.26.

4. Discussion

4.1. Bias Between Eddy Correlation and Chamber Methods

[28] The bias between eddy-correlation and chamber estimates of landscape *ET* in the present study is fairly large. Although some studies have found relatively close (±5%) agreement of chamber fluxes with other methods [*Reicosky and Peters*, 1977; *Reicosky et al.*, 1983; *Pickering et al.*, 1993], other studies have found chambers to be biased high. Chamber *ET* measurements were 25% greater than gravimetric measurements on potted plants [*Grau*, 1995], and 54% greater than Bowen-ratio measurements [*Dugas et al.*, 1997]. The only comparison with eddy-correlation [*Dugas et al.*, 1991] yielded ambiguous results; chamber *ET* was 87% greater, but the chamber measurements were made on the leading edge of a wheat field, where advection probably increased the actual *ET* rate compared to the mid-field EC values. In all of these studies, correlations between methods were high. Our results are well within the range of previous studies, and similarly well correlated, suggesting that although random errors are relatively small, substantial systematic biases between methods are common, and are in need of further attention.

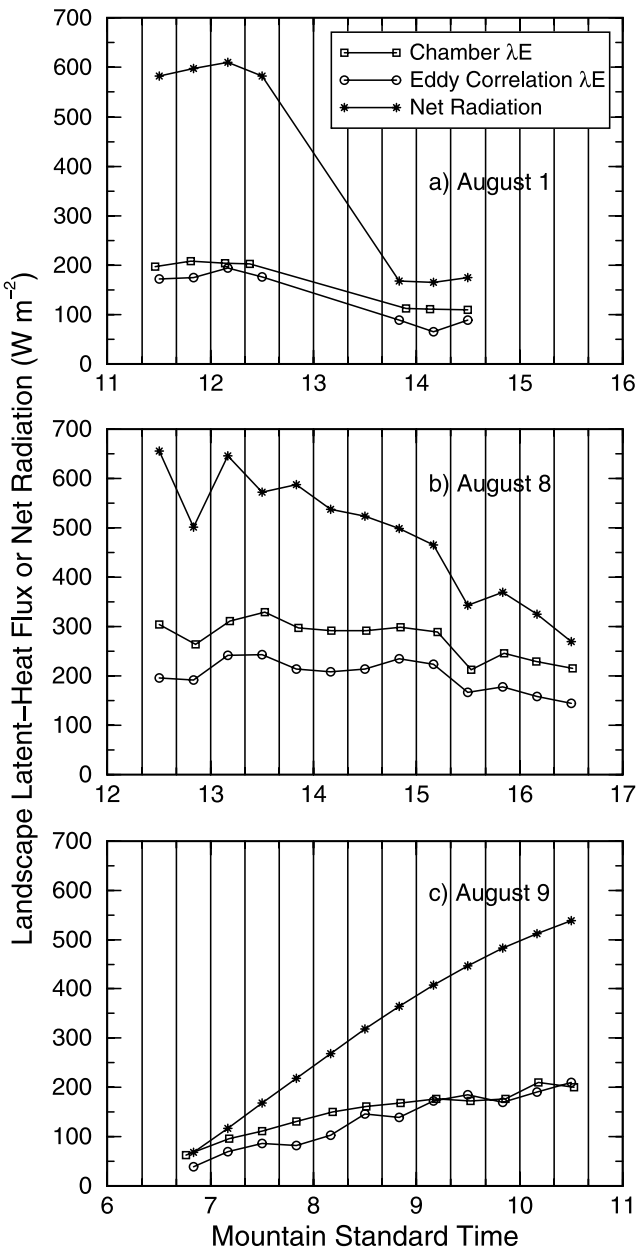

Figure 7. Chamber and eddy-correlation total landscape latent-heat flux and net radiation on (a) August 1, (b) August 8, and (c) August 9.

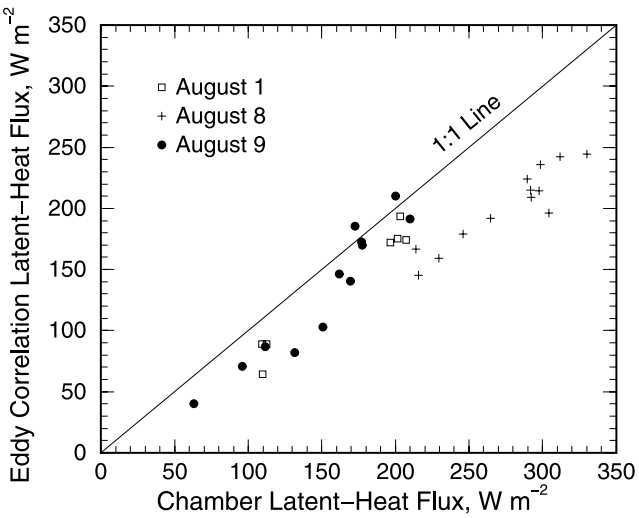

Figure 8. Comparison of chamber and eddy-correlation total landscape latent-heat flux during the study period.

[29] Eddy-correlation measurements of the turbulent sensible- and latent-heat fluxes often sum up to less than the measured available energy (net radiation minus soil-heat flux) [*Twine et al.*, 2000; *Wilson et al.*, 2002; *Brotzge and Crawford*, 2003]. Most researchers agree with *Twine et al.* [2000] that this shortfall indicates the EC method undermeasures the turbulent flux. In the present study, turbulent flux and available energy were highly correlated ($r = 0.96$), and on average, the turbulent flux was 10.2% greater than available energy. This result strongly suggests that the bias between EC and chamber *ET* was not caused by deficiencies in the EC method leading to an under-measurement of *ET*. Rather, the chamber estimates of landscape *ET* probably are biased somewhat high.

[30] The use of chambers often is criticized on the grounds that the internal environment is altered [*Wagner and Reicosky*, 1992; *Denmead et al.*, 1993; *Grau*, 1995; *Dugas et al.*, 1997; *Wagner et al.*, 1997; *Steduto et al.*, 2002; *Heijmans et al.*, 2004], thereby affecting the evaporation rate. Static chambers tend to reduce solar radiation, increase internal temperature and vapor pressure, and alter wind speed. Because this chamber tends to over-measure *ET*, reduced radiation does not appear to be a significant problem. During this study, average measurement time, Δt, (time elapsed between emplacement and the time of measurement, t_m) was 30.2 s, with a standard deviation of 8.9 s. The average increase in chamber temperature during a measurement, ΔT_{ch}, was 1.47°C (std. dev. = 0.77°C) at an average initial temperature of 30.41°C. The average increase in vapor pressure, Δe_{ch}, was 0.26 kPa (std. dev. = 0.16 kPa), at an average initial vapor pressure of 1.68 kPa. These changes in T_{ch} and e_{ch} are consistent with other studies using chambers of a similar size [e.g., *Wagner and Reicosky*, 1992; *Pickering et al.*, 1993]. Individually, they are large enough to alter substantially the vapor-pressure difference that drives *ET* (evaporating-surface vapor pressure minus free-air vapor pressure). Together though, these changes tend to offset one another because both the evaporating-surface and free-air vapor pressures increase. Although we did not measure the evaporating-surface temperature, if we assume a warming rate equal to that of the air, the above data suggest that on average, the vapor-pressure difference driving *ET* was enhanced about 5% during a measurement due to heat and vapor accumulation within the chamber. The alterations to the internal environment that occurred during this study do not appear to be a major factor contributing to the bias between methods.

[31] Some amount of chamber measurement error appears to be related to internal air speed. The bias between EC and chamber estimates of landscape *ET* was substantially greater on August 8 than on the other two days (Figures 7 and 8). The chamber fans were powered by a different type of battery on August 8 that caused the fans to run noticeably faster, and the shrub leaves to be more buffeted. We believe that the greater air speed on August 8 inflated the chamber measurements relative to the other days by increasing the turbulent intensity within the chamber, and reducing the leaf boundary-layer thickness. In addition, we believe the internal air speed was greater than wind speed at chamber height during most of our measurements, causing much of the bias between the estimates of landscape *ET*. However, this bias should be relatively constant between components, causing little error in the computed partitioning. Other studies also have found a relation between air speed and measured flux [*Grau*, 1995; *Dugas et al.*, 1997; *Heijmans et al.*, 2004], although one study found no relation [*Steduto et al.*, 2002].

[32] Use of a canopy model to scale up site measurements also may potentially contribute to the bias in the chamber estimate of landscape *ET*. In particular, the one-layer model used here assigns soil evaporation from under the shrub crown to transpiration, does not account for shading effects, and assumes that leaf area is proportional to shrub plan area. To investigate the effects of the first two assumptions, a two-layer model was developed, which separates crown area soil evaporation from transpiration and accounts for shading effects using standard Sun-Earth geometry and an assumed ratio between shaded and sunlit soil evaporation. These two changes had no effect on computed total landscape *ET*. Regarding the assumed proportionality between leaf area and plan area, analyses of leaf area distribution within the shrub volume and shrub size distributions in the community strongly suggest that the sizes of shrubs selected for measurement in this study would cause, if anything, a slight under-estimate of landscape *ET* using either model. Although we cannot identify a model-induced high bias, the uncertainty involved in scaling measurements made on about 5 m^2 (total chamber area sampled) up to $\sim 10^4$ m^2 (EC source area) may contribute substantially to the bias between methods seen here.

4.2. *ET* Partitioning

[33] To look more closely at partitioning, we define the component fraction of landscape *ET*, $F^i = \lambda E_l^i / \lambda E_{ch}$, where F^i is the fraction of total landscape *ET* contributed by the ith component (species or bare soil), λE_l^i is the landscape-scale latent-heat flux from the ith component, and λE_{ch} is the chamber landscape latent-heat flux. The sum of the vegetation components, including the unmeasured species component, is denoted as F^{vg}, and is equal to $1 - F^{bs}$.

[34] Although model choice (one- or two-layer) does not affect the computed landscape *ET*, it does affect the partitioning between the vegetation and soil components. In the two-layer model, the ratio of shaded to sunlit soil evapora-

Table 2. Standard Deviations and Ranges of *ET* Component Fractions, and Correlation Matrix Between Environmental Variables and Component Fractions

Name of *ET* Component Fraction[a]	Standard Deviation	Range	Plant Height, m	Correlation Coefficient, r (p Value[e])		
				rh_2[b]	T_2[c]	$\theta_{2.5}$[d]
Vegetation, F^{vg}	0.0685	0.360	—	−0.756 (<0.0001)	0.689 (<0.0001)	−0.588 (0.0004)
Bare Soil, F^{bs}	0.0685	0.360	—	0.756 (<0.0001)	−0.689 (<0.0001)	0.588 (0.0004)
Desert Zinnia, F^{dz}	0.0495	0.238	0.1	−0.733 (<0.0001)	0.728 (<0.0001)	−0.426 (0.0151)
Mariola, F^{ma}	0.0037	0.016	0.3	−0.707 (<0.0001)	0.628 (0.0001)	−0.638 (0.0001)
Tar Bush, F^{tb}	0.0128	0.046	0.4	−0.449 (0.0100)	0.255 (0.159)	−0.774 (<0.0001)
Creosote Bush, F^{cb}	0.0107	0.045	0.9	−0.338 (0.0580)	0.182 (0.318)	−0.850 (<0.0001)
White Thorn, F^{wt}	0.0174	0.081	0.4	0.200 (0.271)	−0.122 (0.508)	0.552 (0.0010)

[a]Component fraction is ratio of landscape scale latent-heat flux of a given component to total landscape latent-heat flux (unitless).
[b]Relative humidity at a 2.0-m height (unitless).
[c]Air temperature at a 2.0-m height (°C).
[d]Soil water content at a 2.5-cm depth (m^3 H_2O m^{-3} soil).
[e]Probability that slope of regression is not different than zero.

tion is denoted as C_s. Allowing C_s to vary from 0 to 1 causes mean F^{vg} to vary from 0.865 to 0.782, whereas using the one-layer model, mean $F^{vg} = 0.840$ (Table 1). Setting $C_s = 0.308$ in the two-layer model yields the same partitioning as in the one-layer model. Factors affecting C_s are complex, involving near-surface soil-water content and available energy of shaded and sunlit soil, making accurate estimation of C_s difficult without direct measurement. However, considering that the direct solar beam contains about 70–80% of the total energy in solar radiation [*Monteith and Unsworth*, 1990, Figure 4.7] an estimate of $C_s \cong 0.3$ is plausible, suggesting that little error in partitioning arises from the use of the one-layer model.

[35] The degree of scatter about the best fit lines in Figure 6 suggests that some changes in partitioning occurred during this study. Using the one-layer model, the correlation of partitioning with environmental factors was explored by regressing F^{vg} and F^{i} against all measured and computed temperature-, vapor pressure-, radiation- and soil moisture-related variables, as well as various fluxes and ratios of fluxes. The three most highly correlated variables are presented in Table 2, along with ranges and standard deviation of component fractions. In general, the ranges are about 4 to 5 times the standard deviations, suggesting that the component fraction distributions are roughly normal. Standard deviations of F fall into two distinct groups: large (F^{vg}, F^{bs}, and F^{dz}) and small (F^{ma}, F^{tb}, F^{cb}, and F^{wt}). The standard deviation of a component reflects not only its inherent response to the environment, but also its fractional cover. The F of a species with a very small fractional cover may be highly correlated to environmental changes, but it will still remain relatively constant (i.e., a small standard deviation) simply because it contributes little to the overall landscape *ET*.

[36] Water availability near the soil surface and in the root zone are likely to be important in *ET* partitioning between F^{bs} and F^{vg}. At the study site, no rainfall occurred for 11 days prior to August 1 and for 5 and 6 days prior to August 8 and 9, respectively. As a result, during the measurement days, the shallow soil moisture was relatively low ($0.013 < \theta_{2.5} < 0.047$). In contrast, the root-zone soil moisture, θ_{rz}, was ample, suggesting that the soil component fraction, F^{bs}, is likely to be positively correlated with $\theta_{2.5}$. The correlation is positive (Table 2), but the magnitude is somewhat low ($r = 0.588$). The low correlation probably is partly caused by the small range in $\theta_{2.5}$ (about 0.034), but also suggests that other mechanism(s) may contribute to the soil-vegetation partitioning of *ET*.

[37] At this site, F^{vg} (and F^{bs}) are most highly correlated with relative humidity, rh_2, and air temperature, T_2 (Table 2). A likely explanation for the positive correlation between F^{veg} and T_2 is based on the unique relation between temperature, T, and saturation-vapor pressure, e_s. Both e_s and de_s/dT increase with increasing T. In addition, transpiration is driven by the difference between saturation-vapor pressure at leaf temperature, e_{sl}, and free-air vapor pressure, whereas soil evaporation is driven by the difference between saturation-vapor pressure at the soil-evaporation site temperature, e_{ss}, and free-air vapor pressure. Therefore, if leaf temperature, T_l, is greater than soil evaporation site temperature, T_s, or if T_l varies more widely than T_s with changes in T_2, then F^{vg} will tend to be positively correlated with T_2, and F^{bs} will tend to be negatively correlated. We did not measure leaf or soil evaporation site temperatures, but the large insulating value of a few cm of dry soil suggests that during the day, leaves probably are warmer and thermally more active than the soil evaporation sites, leading to a positive correlation between F^{vg} and T_2. The correlation of F^{vg} with rh_2 (−0.756) is somewhat greater than with T_2 (0.689). At this site, rh_2 and T_2 are highly correlated with one another ($r = 0.971$), suggesting that much of the correlation between F^{vg} and rh_2 may be attributed to the temperature mechanism described here. However, since $VPD = (1 - rh)e_s$, where *VPD* is vapor pressure deficit, the greater correlation in part may be caused by the dependence of stomatal conductance on *VPD* [*Jarvis*, 1976].

[38] Behavior of the individual species component fractions further supports the proposed link between partitioning and temperature. As shown in Figure 9, daytime air temperature decreases nonlinearly with height and temperature profiles are much more active near the surface. Therefore T_l (and corresponding e_{sl}) also is more active near the surface. In general, the degree of correlation between F and T_2 decreases as plant height increases (Table 2). Correlations of the tallest 3 species are not significant at the $p = 0.1$ level, indicating that temperature does not affect partitioning significantly in the upper canopy. This pattern of

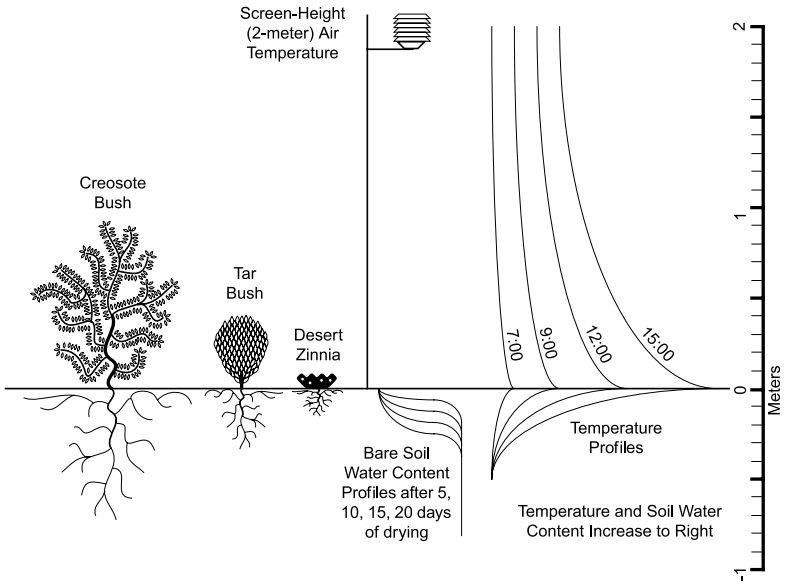

Figure 9. Conceptual model of a mixed height vegetation canopy, showing dependence of temperature-related variability in *ET* partitioning on plant height. Shorter shrubs are thermally more active and contribute more to total *ET* with increasing temperature, at the expense of soil evaporation. Thermal activity of evaporating soil moisture decreases as depth of drying front increases.

decreasing correlation with height supports the premise that leaves closer to the ground undergo greater temperature changes, leading to greater changes in leaf-to-air vapor pressure differences. As with F^{wg}, individual component correlations with rh_2 are greater than with T_2, again possibly indicating changes in stomatal conductance with *VPD*.

[39] Figure 10 shows the variation of the individual component fractions of landscape *ET* as a function of T_2, best fit lines through the data, and the slopes per 10°C. The most notable features of this figure are the "trade-off" between desert zinnia transpiration and soil evaporation as a function of temperature, and the relative constancy of the other components. As temperature increases, the heat generated near the ground is partitioned into desert zinnia transpiration primarily at the expense of soil evaporation. Even though the response of 0.3 m-high mariola is fairly well correlated with T_2 (r = 0.628), the *FC* is so small (0.008) that the resulting contribution to landscape *ET* is fairly constant (slope = 0.013). Creosote bush, white thorn, and tar bush responses are similarly constant (slopes = 0.010, −0.011 and 0.018, respectively), somewhat because of smaller fractional cover (Table 1), but primarily because of small correlations (Table 2). The responses of desert zinnia and bare soil are more than an order of magnitude greater (slopes = 0.196 and −0.257, respectively) than the other components. The overall correlation between F^{veg} and T_2 of 0.689, is now seen to be primarily a result of the high correlation of T_2 with F^{dz}, with minor contributions from tar bush, mariola, and creosote bush, in that order (based on slopes in Figure 10).

[40] Species component fractions (except for white thorn) are negatively correlated with shallow soil moisture ($\theta_{2.5}$) because F^{bs} and $\theta_{2.5}$ are positively correlated (Table 2); i.e., the vegetative correlations essentially are passive in nature. The trend in $F^i - \theta_{2.5}$ correlations with plant height is opposite to the trend in $F^i - T_2$ correlations, increasing in magnitude with plant height (Table 2). This trend probably is related to rooting depth, which, although not measured at this site, tends to mirror plant height (Figure 9). Deeply rooted plants access the more ample, deep soil moisture and therefore respond physiologically very little to changes in $\theta_{2.5}$, allowing the passive correlation to dominate their response. In contrast, shallowly rooted plants probably draw somewhat more on $\theta_{2.5}$, and therefore compete to some degree with soil evaporation, which reduces their negative correlations with $\theta_{2.5}$. White thorn correlations with environmental variables are of opposite sign to the other four species (Table 2). Although white thorn correlations with T_2 and rh_2 are not significant at the $p = 0.05$ level, the correlation with $\theta_{2.5}$ is significant. We can not offer a

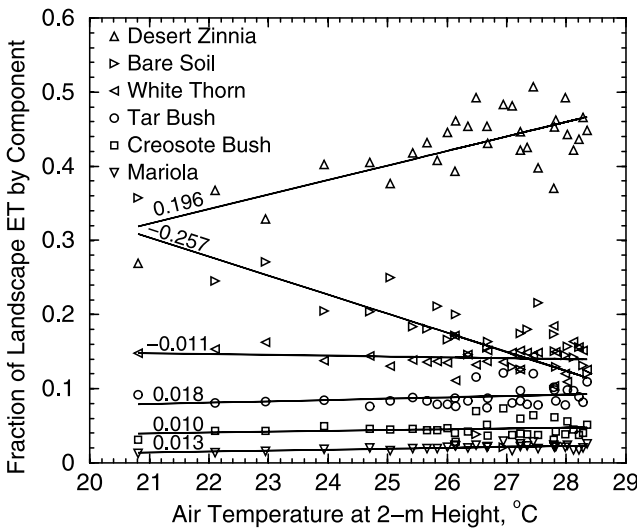

Figure 10. Component fractions of landscape *ET* as a function of air temperature, with best fit lines and slopes per 10°C, of best fit lines.

physical interpretation for this anomalous behavior, and can only speculate that the consistently opposite response of white thorn suggests a possible systematic error in some aspect of the white thorn data collection.

[41] The temperature-soil moisture-plant height relations described here pertain to a relatively narrow range of soil-moisture status, and probably are just a "snapshot" of a larger continuum that changes as soil drying progresses. We propose here a more general description that arises from applying the same height-dependent relations to a full drying cycle. Shortly after a soaking rain, landscape *ET* is dominated by bare-soil evaporation [*Kurc and Small*, 2004], i.e., F^{bs} is a maximum. Also, F^{bs} is positively correlated with T_2 (times -1 for F^{vg}) because the soil evaporation site (the surface) is thermally most active. As the soil dries from the surface downward, the locus of soil evaporation recedes beneath the surface, becoming thermally less active with depth. During this period, F^{bs} decreases, F^{vg} increases, and the correlations of both with T_2 decrease toward zero. When the thermal activity of soil evaporation decreases sufficiently, the lowest layers of vegetation become positively correlated with T_2. As the locus of soil evaporation recedes deeper, the layer of vegetation positively correlated with T_2 grows from the surface upward through the canopy, exhibiting a decreasing correlation with height at any given time. This pattern of T_2 correlations matches the conditions observed during the present study. Now considering correlations between component fractions and $\theta_{2.5}$, during the early stages of soil drying, a strong positive correlation between $\theta_{2.5}$ and F^{bs} (times -1 for F^{vg}) arises from the strong coupling between $\theta_{2.5}$ and the depth of evaporation. As the depth of soil evaporation passes 2.5 cm, correlations decrease as $\theta_{2.5}$ begins to level off and becomes less coupled to the depth of evaporation. Once the depth of evaporation begins to reach the shallowest root depths, the overall decrease in the $\theta_{2.5} - F^{vg}$ correlation is distributed more heavily toward the smaller, shallow-rooted plants, as they begin to compete with soil evaporation for the same water supply. This pattern of $\theta_{2.5}$ correlations also matches the conditions observed during the present study. These matching correlation patterns suggest that the present study took place at about this stage of soil drying, roughly corresponding to the 5–10 day soil moisture profiles in Figure 9. The effects of further drying on partitioning are more complex and depend on patterns of root distributions and feedbacks between water use and stomatal response. However, at this site, desert zinnia probably would be the first species to experience stress because its component-scale water use is the greatest and its rooting depth probably is the shallowest.

[42] Stepwise linear regression was used to determine whether prediction of component fractions from more than one variable could improve upon the correlations in Table 2. All components were regressed onto the three variables in Table 2, and the next three most highly correlated variables. No improvement resulted for each of the five major species; i.e., single variables were adequate. Two variables, rh_2 and SM_5, were significant for prediction of F^{veg} (and F^{bs}), increasing the r^2 from 0.572 (using just rh_2), to 0.647 using both variables. This result appears to reflect the importance of temperature (as expressed through rh_2) to the shorter shrubs, the importance of shallow soil moisture to F^{bs} (and therefore passively to the taller shrubs), and possibly the importance of *VPD* (as expressed through rh_2) to all of the vegetation.

[43] The patterns of correlation observed at this site are not necessarily an exhaustive list of *ET* partitioning dynamics. For example, the discussion of temperature effects has emphasized the link between temperature and source-to-sink vapor pressure differences that drive *ET*. However, leaf- temperature effects on stomatal conductance are well known [*Jarvis*, 1976], and may be included implicitly in the correlations observed here. Root-zone soil moisture, vapor-pressure deficit and solar radiation also are known to affect stomatal conductance [e.g., *Stewart*, 1988]. A comprehensive study of partitioning dynamics would quantify the effects of these variables on stomatal conductance, as well as on source-to-sink differences. In addition, more slowly changing phenological, morphological, and ecological variables may be important on longer time scales.

[44] We applied our partitioning results to data collected by *Kurc and Small* [2004] (hereafter KS) at a site in central New Mexico, similar to our site in several ways. Fractional cover, soils, and climate are similar, both sites experience the same monsoon season, and soil moisture below 10 cm was ample during both studies. KS made Bowen-ratio measurements of *ET* from a creosote-bush monoculture through many monsoon drying cycles during 3 years. They obtained high correlations between the 0–5 cm soil-water content (θ_{0-5}) and both *ET* and *EF* [$EF = \lambda E/(R_n - G)$], low correlations between root-zone soil-water content (θ_{rz}) and both *ET* and *EF*, and documented a lack of roots in the 0–5 cm layer. Based on these observations, KS concluded that "...most of the *ET* at the shrubland must be the result of direct evaporation from the soil." We submit that this evidence does not necessarily identify the overall source of water used for *ET*, just the source of the high- flux events, shortly after rainfalls. We estimated the overall partitioning at the KS site during the 13-day average return interval observed by them for rainfalls >8 mm. We multiplied their mean daily *ET* values during a drying cycle (from KS, Figure 11f) by the partitioning estimated from our study. We used the exponential decay model (KS equation 5) and *ET* time constant (1.9 days) to describe the decreasing soil evaporation fraction, F^{bs}, after a rainfall. We set $F^{bs} = 0.95$ on day 1, and solved for the final value of F^{bs} by fitting the function to our measured F^{bs} on days 5, 6 and 11. Our measured partitioning was computed using our creosote bush and bare soil component-scale fluxes, converted to landscape scale using fractional cover at the KS site (0.30). Using the one-layer model, $F^{vg} = 53.4\%$ during the first 12 days of a dry-down cycle at the KS site (the day of rainfall is excluded, as in KS). Using the two-layer model, F^{vg} varies from 56.2% to 46.9% as the ratio of shaded to sunlit soil evaporation varies from 0 to 1. This example is only approximate, but it suggests that the overall contributions of soil evaporation and transpiration may be about equal during the monsoon. Although the greatest *EF* and *ET* values in KS, Figures 8b and 9 (right, top) probably are derived primarily from θ_{0-5}, leading to the high correlations, these short bursts of soil evaporation are ephemeral, decreasing rapidly as the soil surface dries. In contrast, the shrubs are rooted in the more ample and less variable θ_{rz}, and contribute slowly but steadily to landscape *ET* during

almost the whole drying cycle. The smaller variability of the transpiration stream and its source result in a lower correlation, but the lower correlation does not necessarily imply a smaller flux.

5. Conclusions

[45] Portable closed chamber measurements of evapotranspiration (*ET*) from individual shrubs were made on 3 separate days during a monsoon season in southern Arizona, at periods of 5, 6 and 11 days after substantial rainfalls. The measurements were used successfully in a simple one-layer model [*Stannard*, 1988]of the vegetated land surface to estimate *ET* from each component of the landscape: transpiration from each of the five major species, transpiration from unmeasured species, bare-soil evaporation, and total landscape *ET*. The model represents this sparsely vegetated semiarid site as it would appear in an aerial photograph. The chamber estimates of landscape *ET* were on average 26.5% greater than concurrent eddy-correlation (EC) measurements of landscape *ET* and the two were highly correlated ($r = 0.92$). The most likely sources of bias in the chamber estimates of landscape *ET* appear to be the mismatch of internal air speed with external wind speed, and, to a lesser extent, chamber heating. We believe the air speed problem should be addressed by matching the internal air speed to the external wind speed and developing a chamber analysis routine that accounts for variable internal air speed.

[46] Component-scale *ET* (*ET* per unit horizontal area of component) of vegetation was much greater than that of bare-soil because the soil surface was dry, whereas root-zone soil moisture was ample. Component-scale transpiration, averaged over the study period, ranged from 773 W m^{-2} (desert zinnia) to 312 W m^{-2} (creosote bush), compared to a component-scale bare-soil evaporation of 44 W m^{-2}. Landscape-scale *ET* (*ET* per unit area of landscape) of vegetative components was much less than component-scale *ET* because fractional cover (*FC*) of vegetative components was very small. Landscape scale *ET* of vegetative components ranged from 88 W m^{-2} (desert zinnia) to 4 W m^{-2} (mariola). Consequently, the relative importance of bare soil evaporation increased dramatically at the landscape scale (32 W m^{-2}, second only to desert zinnia) because of its large *FC* (0.737). Even though desert zinnia is the smallest statured species in the community, it accounted for the greatest fraction of landscape *ET* (44%) because of its largest component-scale *ET* and its greatest vegetative abundance ($FC = 0.114$).

[47] Partitioning of landscape *ET* into component fractions (landscape-scale *ET* of a component divided by total landscape *ET*) was somewhat variable during the study. Component fractions were most highly correlated with relative humidity and air temperature at a 2-m height (rh_2 and T_2, respectively). Species component fractions were positively correlated with T_2 (negatively correlated with rh_2) and the degree of correlation generally decreased with increasing plant height. The soil-evaporation fraction was oppositely correlated with these variables. These relations suggest a conceptual model of transpiration driven by the evolution of the curvilinear air-temperature lapse profiles during the day. In a sparse canopy, these profiles are monotonic, increasing in temperature and in slope as height decreases, all the way to the soil surface. In addition, the profiles in general are steeper as ambient temperature (e.g., T_2) increases. This structure results in greater daily temperature swings (thermal activity) as height above the soil surface decreases. The small xeric leaves track air temperature closely and therefore also experience greater activity in sub-stomatal saturation-vapor pressure nearer the ground. Because this vapor pressure drives transpiration, the partitioning of landscape *ET* shifts toward leaves lower in the canopy as ambient temperature increases. Component fractions were somewhat better correlated with rh_2 than with T_2, possibly because *rh* is related to vapor-pressure deficit (*VPD*) and *VPD* often affects stomatal conductance. However, rh_2 and T_2 were highly correlated with one another ($r = -0.971$), making this distinction somewhat tenuous. The negative correlation between the soil evaporation fraction and T_2 suggests that thermal activity at the average depth of soil evaporation during this study was less than that of the vegetation.

[48] Component fractions also were correlated with soil moisture at a 2.5-cm depth ($\theta_{2.5}$). The soil evaporation fraction was positively correlated and species component fractions were negatively correlated, with the exception of white thorn. Species correlations generally decreased with decreasing plant height. The soil surface was dry and the depth of soil-moisture evaporation probably was a few to several cm below the surface during the study. Soil moisture at 10 cm and deeper was ample. These conditions allowed the deeper-rooted vegetation virtually unlimited access to deep soil moisture whereas direct evaporation of shallow soil moisture was somewhat limited. Assuming that rooting depth mirrors plant height, the correlations probably decreased with decreasing plant height because the more shallow-rooted plants draw some portion of their water for transpiration from the same depths that supply soil evaporation.

[49] This study covered a small segment of the full range of soil drying conditions. The patterns that emerged between temperature, soil moisture, and plant height suggest that immediately after a soaking rain, air temperature is positively correlated with the soil evaporation fraction and negatively correlated with the species transpiration fractions, just opposite to the behavior during this study. As the soil dries from the surface down, these correlations decrease toward zero, and continued drying causes the species fractions to become positively correlated, progressing from the shortest to tallest species. When the vegetation fraction as a whole becomes positively correlated with temperature, the soil evaporation fraction correlation necessarily becomes negative. This study took place during this stage of drying, when the correlations of the two shortest species fractions with temperature were substantially positive, the taller species correlations were nearer zero, and the soil evaporation correlation was substantially negative.

[50] We combined our partitioning data with previously published results [*Kurc and Small*, 2004] describing exponential decay patterns of *ET* after rainfall in a similar semiarid monsoonal setting. We propose that *ET* in such a setting may be roughly equally partitioned between transpiration and soil-moisture evaporation. Soil-moisture evaporation far exceeds transpiration immediately after a rainfall, but decreases rapidly to a value less than transpiration after a

few days. Transpiration is much less variable, and the steady accumulation during the rest of the drying cycle effectively offsets the initial burst of soil-moisture evaporation.

[51] **Acknowledgments.** We thank the personnel at the USDA ARS Tombstone Laboratory for their assistance and for the use of the facility during the Monsoon '90 experiment. We are also grateful to personnel from the ARS Southwest Watershed Research Center (SWRC) for the use of their Monsoon '90 data from the Lucky Hills site. We thank B. J. Andraski, R. L. Scott, M. Sugita, and three anonymous reviewers for their helpful comments on the manuscript. Finally, we thank E. P. Weeks for his assistance with chamber deployment and data collection, and A. C. Riggs for the Figure 1 photo. Funding for the SWRC data was from the NASA Interdisciplinary Research Program in the Earth Sciences (number IDP-88-086) and from the Beltsville Area USDA, ARS. Use of trade, firm, or product names in this report is for descriptive purposes only and does not imply endorsement by the U.S. Government.

References

Brotzge, J. A., and K. C. Crawford (2003), Examination of the surface energy budget: A comparison of eddy correlation and Bowen ratio measurement systems, *J. Hydrometeorol.*, *4*(2), 160–178.

Canfield, R. H. (1941), Application of the line interception method in sampling range vegetation, *J. For.*, *39*, 388–394.

Decker, J. P., W. G. Gaylor, and F. D. Cole (1962), Measuring transpiration of undisturbed tamarisk shrubs, *Plant Physiol.*, *37*, 393–397.

Denmead, O. T., F. X. Dunin, S. C. Wong, and E. A. N. Greenwood (1993), Measuring water use efficiency of Eucalypt trees with chambers and micrometeorological techniques, *J. Hydrol.*, *150*, 649–664.

Dugas, W. A., L. J. Fritschen, L. W. Gay, A. A. Held, A. D. Matthias, D. C. Reicosky, P. Steduto, and J. L. Steiner (1991), Bowen ratio, eddy correlation, and portable chamber measurements of sensible and latent heat flux over irrigated spring wheat, *Agric. For. Meteorol.*, *56*, 1–20.

Dugas, W. A., D. C. Reicosky, and J. R. Kiniry (1997), Chamber and micrometeorological measurements of CO_2 and H_2O fluxes for three C4 grasses, *Agric. For. Meteorol.*, *83*, 113–133.

Fuchs, M., and C. B. Tanner (1968), Calibration and field test of soil heat flux plates, *Soil Sci. Soc. Am. Proc.*, *32*, 326–328.

Goodrich, D. C., T. J. Schmugge, T. J. Jackson, C. L. Unkrich, T. O. Keefer, R. Parry, L. B. Bach, and S. A. Amer (1994), Runoff simulation sensitivity to remotely sensed initial soil water content, *Water Resour. Res.*, *30*(5), 1393–1405.

Grau, A. (1995), A closed chamber technique for field measurement of gas exchange of forage canopies, *N. Z. J. Agric. Res.*, *38*, 71–77.

Heijmans, M. M. P. D., W. J. Arp, and F. S. Chapin III (2004), Carbon dioxide and water vapour exchange from understory species in boreal forest, *Agric. For. Meteorol.*, *123*, 135–147.

Jarvis, P. G. (1976), The interpretation of the variations in leaf water potential and stomatal conductance found in canopies in the field, *Philos. Trans. R. Soc. London, Ser. B*, *273*, 593–610.

Kurc, S. A., and E. E. Small (2004), Dynamics of evapotranspiration in semiarid grassland and shrubland ecosystems during the summer monsoon season, central New Mexico, *Water Resour. Res.*, *40*, W09305, doi:10.1029/2004WR003068.

Kustas, W. P., and D. C. Goodrich (1994), Preface, *Water Resour. Res.*, *30*(5), 1211–1225.

Kustas, W. P., J. H. Blanford, D. I. Stannard, C. S. T. Daughtry, W. D. Nichols, and M. A. Weltz (1994), Local energy flux estimates for unstable conditions using variance data in semiarid rangelands, *Water Resour. Res.*, *30*(5), 1351–1361.

Monteith, J. L., and M. H. Unsworth (1990), *Principles of Environmental Physics*, Edward Arnold, London.

Pickering, N. B., J. W. Jones, and K. J. Boote (1993), Evaluation of the portable chamber technique for measuring canopy gas exchange by crops, *Agric. For. Meteorol.*, *63*, 239–254.

Reicosky, D. C., and D. B. Peters (1977), A portable chamber for rapid evapotranspiration measurements on field plots, *Agron. J.*, *69*, 729–732.

Reicosky, D. C., B. S. Sharratt, J. E. Ljungkull, and D. G. Baker (1983), Comparison of alfalfa evapotranspiration measured by a weighing lysimeter and a portable chamber, *Agric. Meteorol.*, *28*, 205–211.

Reifsnyder, W. E. (1967), Radiation geometry in the measurement and interpretation of radiation balance, *Agric. Meteorol.*, *4*, 255–265.

Schmugge, T., T. J. Jackson, W. P. Kustas, R. Roberts, R. Parry, D. C. Goodrich, S. A. Amer, and M. A. Weltz (1994), Push broom microwave radiometer observations of surface soil moisture in Monsoon '90, *Water Resour. Res.*, *30*(5), 1321–1327.

Schuepp, P. H., M. Y. LeClerc, J. I. MacPherson, and R. L. Desjardins (1990), Footprint predictions of scalar fluxes from analytical solutions of the diffusion equation, *Boundary Layer Meteorol.*, *50*, 355–373.

Stannard, D. I. (1988), Use of a hemispherical chamber for measurement of evapotranspiration, *U.S. Geol. Surv. Open File Rep.*, *88-452*, 18 pp.

Stannard, D. I., J. H. Blanford, W. P. Kustas, W. D. Nichols, S. A. Amer, T. J. Schmugge, and M. A. Weltz (1994), Interpretation of surface flux measurements in heterogeneous terrain during the Monsoon '90 experiment, *Water Resour. Res.*, *30*(5), 1227–1239.

Steduto, P., O. Cetinkoku, R. Albrizio, and R. Kanber (2002), Automated closed-system canopy- chamber for continuous field-crop monitoring of CO_2 and H_2O fluxes, *Agric. For. Meteorol.*, *111*, 171–186.

Stewart, J. B. (1988), Modelling surface conductance of pine forest, *Agric. For. Meteorol.*, *43*, 19–35.

Twine, T. E., et al. (2000), Correcting eddy-covariance flux underestimates over a grassland, *Agric. For. Meteorol.*, *103*, 279–300.

Wagner, S. W., and D. C. Reicosky (1992), Closed-chamber effects on leaf temperature, canopy photosynthesis, and evapotranspiration, *Agron. J.*, *84*, 731–738.

Wagner, S. W., D. C. Reicosky, and R. S. Alessi (1997), Regression models for calculating gas fluxes measured with a closed chamber, *Agron. J.*, *89*, 279–284.

Weltz, M. A., J. C. Ritchie, and H. D. Fox (1994), Comparison of laser and field measurements of vegetation height and canopy cover, *Water Resour. Res.*, *30*(5), 1311–1319.

Wilson, K. A., et al. (2002), Energy balance closure at FLUXNET sites, *Agric. For. Meteorol.*, *113*, 223–243.

D. I. Stannard, Water Resources Division, U.S. Geological Survey, MS 413, Denver, CO 80225, USA. (distanna@usgs.gov)

M. A. Weltz, Agricultural Research Service, U.S. Department of Agriculture, Beltsville, MD 20705, USA.